

A search for heavy Kaluza-Klein electroweak gauge bosons at the LHC

Gideon Bella, Erez Etzion, Noam Hod, Yaron Oz, Yiftah Silver

*The Raymond and Beverly Sackler School of Physics and Astronomy, Tel-Aviv
University
E-mail: noam.hod@cern.ch*

Mark Sutton

*The Department of Physics and Astronomy, University of Sheffield
E-mail: sutt@cern.ch*

ABSTRACT: The feasibility for the observation of a certain leptonic Kaluza-Klein (KK) hard process in pp interactions at the LHC is presented. Within the S^1/Z_2 TeV^{-1} extra dimensional theoretical framework with the focus on the KK excitations of the Standard Model γ and Z^0 gauge bosons, the hard-process, $f\bar{f} \rightarrow \sum_n (\gamma^*/Z^*)_n \rightarrow F\bar{F}$, has been used where f is the initial state parton, F the final state lepton and $(\gamma^*/Z^*)_n$ is the n^{th} KK excitation of the γ/Z^0 boson. For this study the analytic form for the hard process cross section has been independently calculated by the authors and has been implemented using the MOSES framework. The Moses framework itself, that has been written by the authors, was used as an external process within the PYTHIA8 Monte Carlo generator which provides the phase space generation for the final state leptons and partons from the initial state hadrons, and the simulation of initial and final state radiation and hadronization. A brief discussion of the possibility for observing and identifying the unique signature of the KK signal given the current LHC program is also presented.

KEYWORDS: Beyond the Standard Model, Heavy Gauge Bosons, Extra Dimensions, Kaluza-Klein, LHC.

Contents

1. Introduction	1
2. The general Kaluza-Klein hard process at leading order	2
3. The KK signal at the LHC	4
4. The LHC sensitivity for the KK signal	9
5. Summary and Outlook	14
6. Acknowledgments	15

1. Introduction

Several theories [1, 2, 3, 4] predict the existence of extra dimensions (ED) in addition to the usual three spatial and one time dimension. These models allow various particles to propagate into the extra-dimensional bulk. In this paper a model [4, 5] where a single extra spatial dimension is compactified onto an S^1/Z_2 orbifold is considered, where the radius of the S^1 -shaped extra dimension is denoted by R .

This model allows the KK modes of $SU(2) \times U(1)$ gauge fields to propagate into the extra-dimensional bulk, while restricting all the matter fermions to be localized in the usual three space dimensions [1, 2, 6]. The process discussed in this paper is of particular interest in the context of physics at the LHC [7], since the signal, unlike other possible heavy Z -like signals, such as the Z' , manifests a strong destructive interference between the KK and the Standard Model (SM) states at invariant-masses much lower than the mass of the first KK resonance itself. Even for a resonance around ~ 4 TeV, this suppression is expected to be within the reach of the LHC and it could be observed relatively early during LHC operation [8, 9, 10].

For this paper, the analytic form [9] for the cross section of the $f\bar{f} \rightarrow \sum_n (\gamma^*/Z^*)_n \rightarrow F\bar{F}$ hard process has been independently verified at leading order by the authors. For the subsequent studies, fully simulated events at the hadron level have been produced using the MOSES framework [11] for the generation of the hard subprocess which has been implemented as an external process within the PYTHIA8 Monte Carlo generator [12]. All the stages in the event simulation not involved in the hard subprocess generation, *ie* initial and final state radiation (ISR and FSR), generation of the partons kinematics for the incoming beam protons, parton showering, hadronization, proton remnant fragmentation and particle decay etc. are performed by PYTHIA8.

In a previous study [14] for this KK process the matrix elements were interfaced to the FORTRAN PYTHIA-v6 and the generated events passed through the fast simulation [15] of the ATLAS detector [16], assuming proton-proton interactions at $\sqrt{s}_{\text{LHC}}=14$ TeV centre-of-mass energy, integrated LHC luminosity, $\mathcal{L}_{\text{LHC}}=100 \text{ fb}^{-1}$, and a KK resonance mass of $m_{Z^*} = 4$ TeV. Previous studies of the possible Z' signal at the LHC have also been performed [17].

This paper replicates aspects of the previous study with independently verified Matrix Elements and also considers the additional model which assumes the existence of an extra heavy, Z' , boson arising from a spontaneous breaking of a higher gauge symmetry group [8, 13]. In this additional model, Z' bosons can be produced with different couplings. One scenario often introduced is the Z'_{SM} where the new boson has the same couplings as the Z^0 but with different mass and width. While there is no theoretical preference for the choice of SM-like couplings for the Z' , distinguishing between the KK and Z' cases where the couplings are SM-like is experimentally more challenging.

In addition, a new quantitative analysis of several Monte Carlo pseudo-data sets, generated using MOSES and PYTHIA8, is presented in order to study the discovery potential for the observation of heavy Kaluza-Klein gauge bosons as a consequence of recent expected early LHC running scenarios. In contrast to the previous study [14] which concentrated on masses around a resonance at 4 TeV, with 14 TeV centre-of-mass energy and a large integrated luminosity of 100 fb^{-1} , this analysis also considers the effect of the lower 7 TeV centre-of-mass energy and the reduced assumed integrated luminosity of 10 fb^{-1} to ascertain what can be achieved using the lower invariant mass region below the resonance, accessible with the early running scenarios. The effects of initial and final state radiation from the incoming partons or outgoing leptons are also discussed.

2. The general Kaluza-Klein hard process at leading order

For this study the process $q\bar{q} \rightarrow \sum_n (\gamma^*/Z^*)_n \rightarrow l\bar{l}$ was implemented in C++ where q and \bar{q} are incoming quark and anti quark, and l and \bar{l} are outgoing leptons, however, for generality, the following discussion is presented in terms of $f\bar{f}$ and $F\bar{F}$ where $f(F)$ can be any SM initial (final) state fermion. At tree-level, the formulation for the differential cross section for the process $f\bar{f} \rightarrow \sum_n (\gamma^*/Z^*)_n \rightarrow F\bar{F}$ can be written as

$$\frac{d\hat{\sigma}(\hat{s})}{d\cos\theta^*} = 2\pi \frac{\alpha_{\text{em}}^2}{4\hat{s}} \frac{N_C^F}{N_C^f} \frac{\hat{s}^2}{4} \sum_{\lambda_f=\pm\frac{1}{2}} \sum_{\lambda_F=\pm\frac{1}{2}} \left| \sum_{n=0}^{\infty} M_{\lambda_f\lambda_F}^{(n)} \right|^2 (1 + 4\lambda_f\lambda_F \cos\theta^*)^2 \quad (2.1)$$

where \hat{s} is the squared invariant mass of the $q\bar{q}$ state, $N_C^{f(F)}$ is the number of colors of $f(F)$, $\lambda_{f(F)}$ is the helicity of the $f(F)$ fermion and $\cos\theta^*$ is the cosine of the scattering angle with respect to the incoming fermion direction of the outgoing fermions in the $f\bar{f}$ rest frame. The complete amplitude consists of an infinite tower of Kaluza-Klein excitations with increasing mass,

$$\sum_{n=0}^{\infty} M_{\lambda_f\lambda_F}^{(n)} \equiv M_{\lambda_f\lambda_F} + \sum_{n=1}^{\infty} M_{\lambda_f\lambda_F}^{(n)}, \quad (2.2)$$

where the SM term ($n = 0$) is,

$$M_{\lambda_f \lambda_F} \equiv \frac{e_f e_F}{\hat{s}} + \frac{g_{\lambda_f} g_{\lambda_F}}{\hat{s} - m_{Z^0}^2 + i\hat{s} \frac{\Gamma_{Z^0}}{m_{Z^0}}}, \quad (2.3)$$

and the contribution of the n^{th} excitation for $n = 1, 2, 3, \dots$ can be written as,

$$M_{\lambda_f \lambda_F}^{(n>0)}(\hat{s}) \equiv \frac{e_f^{(n)} e_F^{(n)}}{\hat{s} - \left(m_{\gamma^*}^{(n)}\right)^2 + i\hat{s} \frac{\Gamma_{\gamma^*}^{(n)}}{m_{\gamma^*}^{(n)}}} + \frac{g_{\lambda_f}^{(n)} g_{\lambda_F}^{(n)}}{\hat{s} - \left(m_{Z^*}^{(n)}\right)^2 + i\hat{s} \frac{\Gamma_{Z^*}^{(n)}}{m_{Z^*}^{(n)}}}. \quad (2.4)$$

The SM helicity couplings [18] of the Z^0 to the incoming and outgoing fermions are,

$$g_{\lambda_f} = \begin{cases} -\frac{e_f \sin^2 \theta_W}{\sin \theta_W \cos \theta_W} & \text{for } \lambda_f = +\frac{1}{2} \\ \frac{I_f^3 - e_f \sin^2 \theta_W}{\sin \theta_W \cos \theta_W} & \text{for } \lambda_f = -\frac{1}{2} \end{cases} \quad (2.5)$$

where the couplings of the KK states to fermions are larger than their SM counterparts (equation 2.5) by a factor of $\sqrt{2}$ [14, 19]. The n^{th} KK excitation masses $m_{Z^*}^{(n)}$ and $m_{\gamma^*}^{(n)}$ are given by,

$$\begin{aligned} m_{Z^*}^{(n)} &= \sqrt{m_{Z^0}^2 + (n \cdot m^*)^2} \\ m_{\gamma^*}^{(n)} &= n \cdot m^*. \end{aligned} \quad (2.6)$$

where the KK mass, m^* , is dependent on the extra dimension size, R , through the relation $m^* \equiv R^{-1}$. The current, indirectly obtained theoretical lower bound for m^* assuming that there are no other beyond-the-SM (BSM) effects besides the KK model, is around 4 TeV [14, 20, 21]. The total decay width of the KK Z^* appearing in Eq 2.4, is given by,

$$\Gamma_{Z^*}^{(n)} = \Gamma_{Z^0} \times 2 \frac{m_{Z^*}^{(n)}}{m_{Z^0}} + \Gamma_{Z^* \rightarrow t\bar{t}}^{(n)}, \quad (2.7)$$

where $\Gamma_{Z^* \rightarrow t\bar{t}}^{(n)}$ is calculated separately due to the mass of the top quark,

$$\Gamma_{Z^* \rightarrow t\bar{t}}^{(n)} = 2 \frac{N_C^t G_\mu m_{Z^0}^2 m_{Z^*}^{(n)}}{24\pi\sqrt{2}} \left[1 - \frac{4m_t^2}{\left(m_{Z^*}^{(n)}\right)^2} \right]^{\frac{1}{2}} \quad (2.8)$$

$$\times \left[1 - \frac{4m_t^2}{\left(m_{Z^*}^{(n)}\right)^2} + (2I_t^3 - 4e_t \sin^2 \theta_W)^2 \left(1 + \frac{2m_t^2}{\left(m_{Z^*}^{(n)}\right)^2} \right) \right] \quad (2.9)$$

The total decay width of the (massive) KK γ^* appearing in Eq 2.4, is,

$$\Gamma_{\gamma^*}^{(n)} = \sum_{F \neq t} \frac{N_C^F \alpha_{\text{em}} m_{\gamma^*}^{(n)}}{6} \times \left\{ \begin{array}{l} 0 \text{ for } n = 0 \\ 4e_F^2 \text{ otherwise} \end{array} \right\} + \Gamma_{\gamma^* \rightarrow t\bar{t}}^{(n)}, \quad (2.10)$$

where the sum is over all the fermionic decay channels, $F\bar{F}$ except for $t\bar{t}$, assuming SM channels only and where $\Gamma_{\gamma^* \rightarrow t\bar{t}}^{(n)}$ is,

$$\Gamma_{\gamma^* \rightarrow t\bar{t}}^{(n)} = 2 \frac{\alpha_{\text{em}} N_C^t m_{\gamma^*}^{(n)}}{6} 2e_t^2 \left[1 - \frac{4m_t^2}{(m_{\gamma^*}^{(n)})^2} \right]^{\frac{1}{2}} \left[1 + \frac{2m_t^2}{(m_{\gamma^*}^{(n)})^2} \right] \quad (2.11)$$

Equations 2.1 and 2.2 represent a large tower of interfering contributions at increasing masses and is illustrated in figure 1.

$$\sum_{n=0}^{\infty} M_{\lambda_f \lambda_F}^{(n)} = \begin{array}{cccc} (n=0) & & (n=1) & \\ m_{\gamma}^{(0)} = 0 & m_{Z^0}^{(0)} = m_{Z^0} & m_{\gamma^*}^{(1)} = m^* & m_{Z^*}^{(1)} = \sqrt{m_{Z^0}^2 + m^{*2}} \\ \begin{array}{c} \bar{f} \\ \downarrow \\ e_f \text{---} \gamma \text{---} e_F \\ \uparrow \\ f \end{array} & + & \begin{array}{c} \bar{f} \\ \downarrow \\ g_{\lambda_f} \text{---} Z^0 \text{---} g_{\lambda_F} \\ \uparrow \\ f \end{array} & + & \begin{array}{c} \bar{f} \\ \downarrow \\ \sqrt{2}e_f \text{---} \gamma^* \text{---} \sqrt{2}e_F \\ \uparrow \\ f \end{array} & + & \begin{array}{c} \bar{f} \\ \downarrow \\ \sqrt{2}g_{\lambda_f} \text{---} Z^* \text{---} \sqrt{2}g_{\lambda_F} \\ \uparrow \\ f \end{array} & + & \dots \end{array}$$

Figure 1: The Feynman diagram of the entire KK tower of the γ/Z^0 gauge bosons.

For the remainder of this paper, only the di-muon final state is considered so the index F shall be replaced by μ^- .

3. The KK signal at the LHC

The KK processes considered here, $pp \rightarrow \{\gamma/Z^0, Z'_{\text{SM}} \text{ or } \sum_n (\gamma^*/Z^*)_n\} \rightarrow \mu^+ \mu^-$ exhibits several outstanding characteristics that can provide a strong suggestion of the presence of the first KK resonance even before it is directly seen [10]. These characteristics also enable discrimination between other similar possible signals, such as the Z'_{SM} , assuming that the signal can be directly observed [11, 22]. In this paper an attempt is made to address the applicability of such statements in the light of the likely running scenario for the updated LHC schedule in terms of the available collider centre-of-mass energy and the luminosity.

The next-to-leading order (NLO) corrections to Z' production have recently been calculated [24] and have been shown to be around 25% of the leading order contribution. Since the vector-axial vector couplings of the standard model, KK and Z' bosons are all proportional, it might be expected that the NLO correction to the KK signal is also of the same magnitude and an NLO K-factor of 1.25 to scale the leading order cross section to that predicted by the full NLO prediction could be applied. Since applying such an overall factor after generation of events, will not affect the statistical precision of the predictions such a correction has not been applied to any Monte Carlo predictions of the cross section, but it should be noted that any observed signal in the data, might be expected to be 25% higher than the Monte Carlo predictions presented here.

The principal difference between all the Z' models and the KK model is the lack of a heavy photon in the Z' models. The missing interference terms of such a heavy photon in the Standard Model and Z' amplitudes modify the $\sqrt{\hat{s}}(\mu^+ \mu^-)$, $p_T(\mu^-)$ and $\cos \theta^*$ distributions. Although the Z'_{SM} choice is not theoretically preferred, it is in practice the

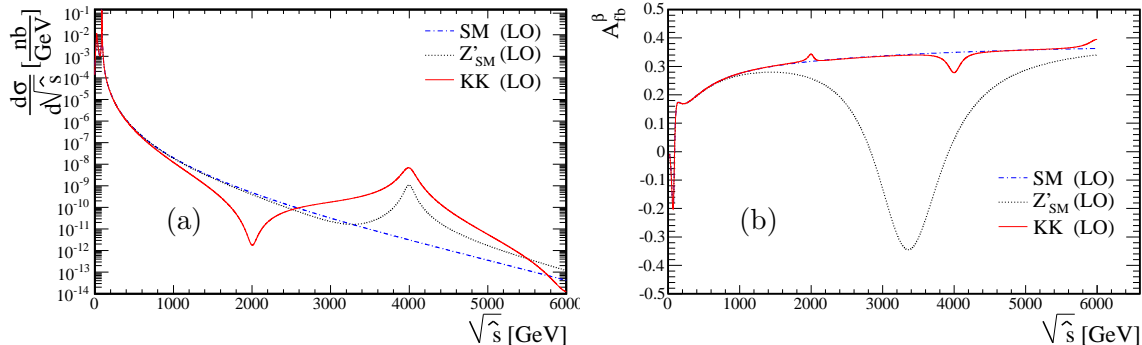


Figure 2: The leading order (LO) invariant-mass distribution (a) and the Forward-Backward asymmetry (b) for the three models, KK (solid), Z'_{SM} (dotted) and SM (dash-dot) discussed in the text.

most challenging for comparison. A study [23] of the relevant Z' scenarios suggests that while they behave similarly at invariant masses below the resonance, those resonances with the non SM couplings are in general narrower and smaller than the Z'_{SM} which is already narrower and smaller than the KK resonance. Moreover, as with the KK resonance, the Z'_{SM} also introduces a suppression of the cross section at invariant masses below the resonance - although this suppression is small - whereas the other Z' scenarios do not [23]. Therefore, since it is the closest in shape to the rather wide KK resonance, the case where the couplings of the Z' are SM-like, will be the most difficult to distinguish from the KK case.

For the remainder of this section, an overview of these characteristics is given for $\sqrt{s}_{LHC} = 14$ TeV and for a KK m^* or Z'_{SM} mass of 4 TeV. All the results will be given within the acceptance for the typical general purpose LHC detector and trigger for muons, *ie*, $p_T > 10$ GeV, $|\eta| < 2.5$. For illustrative purposes, large Monte Carlo reference samples were generated using MOSES and PYTHIA8 to the level of the full, final state hadrons, for each of the SM, Z'_{SM} , and KK models. Samples corresponding to an LHC integrated luminosity of 100 fb^{-1} were also produced. A discussion in the context of the lower LHC centre-of-mass energy, and lower integrated luminosity of the initial LHC running programme with various values of the KK mass parameter, m^* , is given in section 4.

At least three unique signal characteristics of the KK process with respect to either the SM or the Z'_{SM} model can be derived from the di-muon invariant mass distribution (line-shape), the muon p_T and $\cos \theta^*$ distributions.

The invariant mass distributions of the three models can be seen in figure 2(a) for the nominal signal masses of 4 TeV mentioned earlier. The strong suppression of the cross section for the KK line-shape with respect to the SM is clearly seen for masses below half the mass of the first KK resonance. Note that the Z'_{SM} does not differ from the SM line-shape as strongly as the KK line-shape and that this difference is generally to increase the cross section with respect to the SM expectation.

From the $\cos \theta^*$ distribution a clear difference can be seen between the KK and the

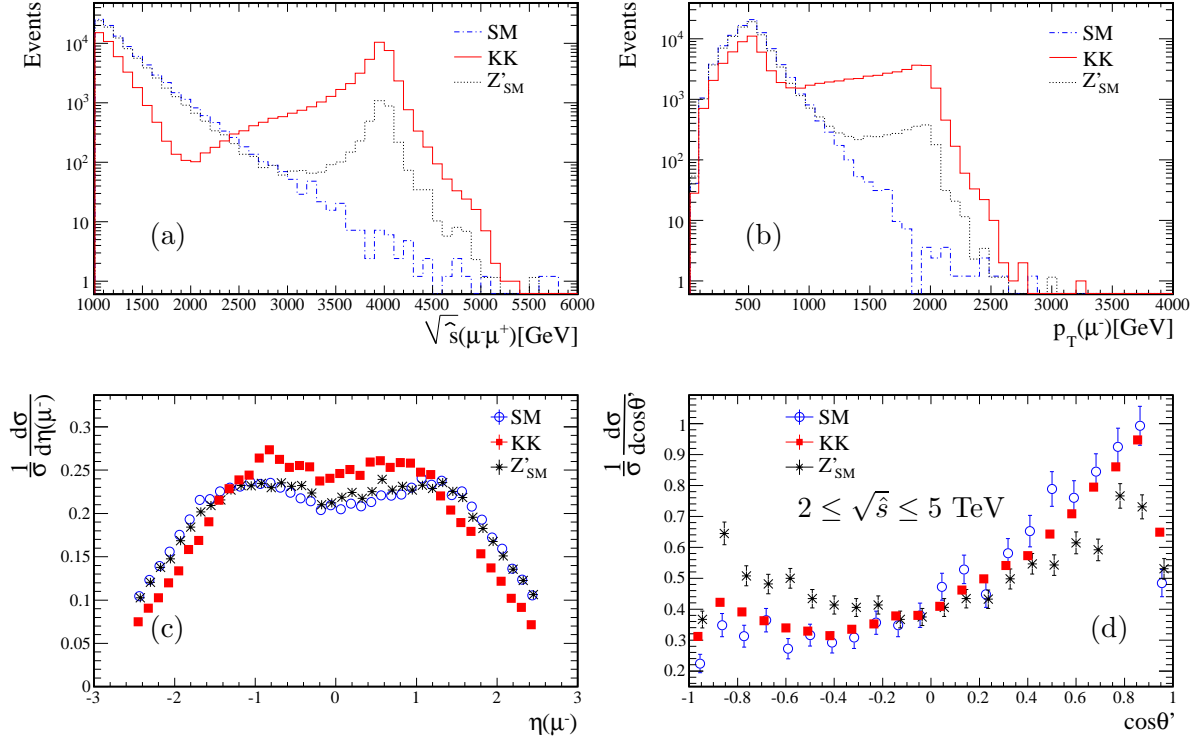


Figure 3: Kinematic distributions of the Monte Carlo reference samples for the KK (solid), the SM (dash-dot) and the Z'_{SM} (dotted) models; (a) The di-muon invariant mass, $\sqrt{\hat{s}}(\mu^+\mu^-)$, (b) the muon p_T spectrum, (c) the muon normalised η distribution, (d) the normalised muon $\cos\theta'$ distribution. An additional requirement of $2 \leq \sqrt{\hat{s}}(\mu^+\mu^-) \leq 5$ TeV has been applied to the events in (d) since the forward-backward asymmetry exhibits a strong dependence on the invariant mass (see figure 2).

Z'_{SM} forward-backward asymmetries, A_{fb} , defined as

$$A_{fb} \equiv \frac{N_f - N_b}{N_f + N_b} \quad (3.1)$$

where N_f and N_b are the number of events before the acceptance cuts on the outgoing leptons, for which respectively, $\cos\theta^* > 0$ (forward) and $\cos\theta^* < 0$ (backward).

Due to the symmetry of the LHC beams, it is not known which beam proton contains the incoming quark and which the anti-quark, so $\cos\theta^*$ cannot be measured with respect to the incoming quark direction. Hence for a meaningful definition of the asymmetry, some event-by-event definition of direction with respect to which the angle of the outgoing muon is measured must be adopted. At leading order the di-muon boost direction will in general coincide with that of the incoming quark along the z direction since the valence quarks are, on average, more energetic than the anti-quarks which originate entirely from the sea. As such, the asymmetry, A_{fb}^β , is defined, measured with respect to the di-muon boost direction, $\vec{\beta}$, in the lab frame. Under this definition, $\cos\theta_\beta^*$ is now the cosine of the angle between the outgoing muon and the boost direction.

The theoretical asymmetry, A_{fb}^β , as a function of the di-muon invariant mass of the three processes can be seen in figure 2(b) and shows a clear difference between the KK and

the Z'_{SM} asymmetries around the 4 TeV mass of the simulated signal states.

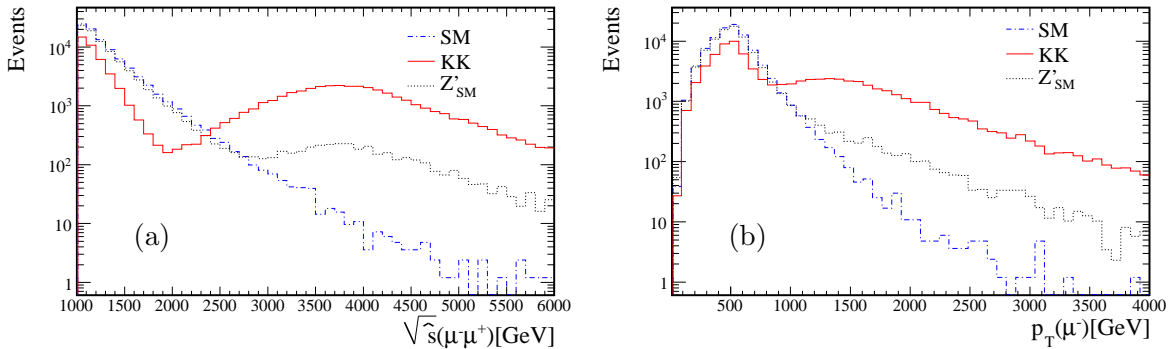


Figure 4: Kinematic distributions of the Monte Carlo reference samples for the KK (solid), the SM (dash-dot) and the Z'_{SM} (dotted) models when including smearing to simulate realistic momentum resolution at the detector level; (a) The reconstructed di-muon invariant mass, $\sqrt{\hat{s}}(\mu^+\mu^-)$ (b) the reconstructed muon p_T spectrum.

Radiation from the initial state partons or the final state leptons will in general lead to the correspondence between the boost direction of the di-muon system and the quark direction being lost to some degree since the di-muon state itself can obtain some transverse momentum with respect to the beam line. As such, it may be better to measure $\cos\theta^*$ in the Collins-Soper frame [25] where the \hat{z} axis is defined along the bisector of the beam directions in the di-lepton rest frame, with the positive direction taken as that closer to $\vec{\beta}$. In this frame, the angle of the muon with respect to the positive \hat{z} axis is denoted by θ' .

The differential distributions for the large reference Monte Carlo samples of the processes implemented using MOSES and PYTHIA8 can be seen in figure 3 where events were generated using the MRST parton distribution set [26]. The invariant mass distribution for each of the three models is shown in figure 3(a), the muon transverse momentum and pseudorapidity distributions are shown in figures 3(b) and 3(c) and finally the distribution of $\cos\theta'$ is shown in figure 3(d). To enhance the forward-backward asymmetry, for the events in figure 3(d), an addition requirement of $2 \leq \sqrt{\hat{s}}(\mu^+\mu^-) \leq 5$ TeV has been applied.

In the distribution with respect to p_T , a significant enhancement can be seen above the SM expectation for transverse momenta around 2 TeV for both the KK and Z'_{SM} models. However, the p_T enhancement for the KK process begins approximately 500 GeV before that from the Z'_{SM} and it is significantly larger.

In the kinematic region around the potential signal states, the large invariant mass of the lepton pair resulting from the decay of the heavy state, will in general result in each lepton possessing a very large transverse momentum. Since the mass reconstruction of the intermediate state is dependent on the muon reconstruction it will in general be less precisely measured for muons with high transverse momentum.

In order to study the effect on the observation of any potential signal resulting from the finite detector resolution the outgoing muon momentum has been smeared by

$$\sigma(p_T) = 0.12 \cdot p_T[\text{TeV}]$$

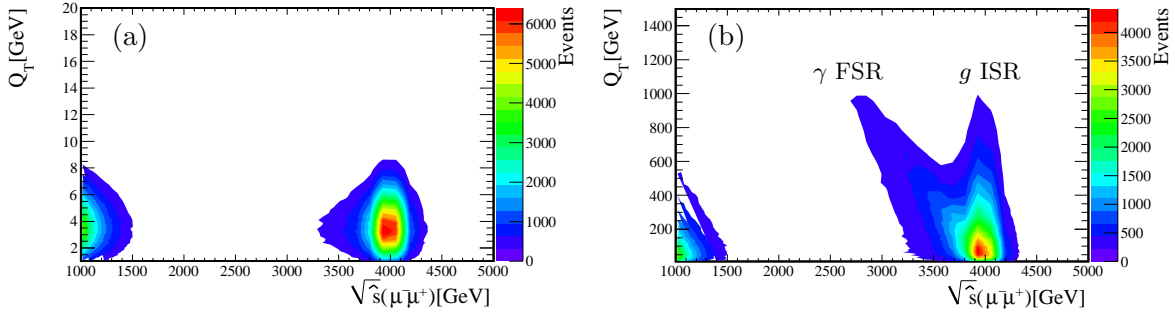


Figure 5: The distribution of the transverse momentum of the di-muon state, Q_T versus the di-muon invariant mass, $\sqrt{\hat{s}}$. In (a), the initial- and final-state radiation in PYTHIA8 is switched off, whereas in (b) it is switched on. Note the larger scale for the y-axis in (b).

typical of the resolution obtainable by either the ATLAS or CMS experiments [27, 28] for ~ 1 TeV muon tracks. The reconstructed invariant and transverse momentum distributions for “reconstructed” detector level muons can be seen in figure 4, after the same “true” tracks used to obtain the distributions seen in figure 3, had been smeared. In this case, clearly the invariant mass peaks and the enhancement in the transverse momentum distribution have been greatly smeared, notably in the very high invariant masses or transverse momenta, although the characteristic valley in the invariant mass distribution is clearly seen.

In PYTHIA8, the effects of initial and final state radiation from the incoming partons or outgoing muons can be easily controlled by switches. Their influence on the di-muon system, can be seen by considering the transverse momentum, Q_T , of the di-muon system. Figure 5 shows the the distribution of Q_T versus the di-muon invariant mass, $\sqrt{\hat{s}}(\mu^+\mu^-)$ for the case where initial- and final-state radiation is switched off, figure 5(a) and where they are both switched on, figure 5(b). This clearly shows that for the case where an initial parton has radiated the di-muon system will in general be boosted in the transverse plane to balance the radiation for any given di-muon invariant mass. For the case of radiation from one of the final state leptons, the intermediate state will not in general have significant transverse momentum but the di-muon state itself will be balanced by the transverse momentum of the radiated photon which may not be observed or associated with the di-muon system.

Both of these effects will therefore have an impact on the $\cos\theta_\beta^*$ and p_T distributions. Radiation of a final state photon which is not reconstructed as part of the di-muon system will give rise to a reduction of the measured di-muon invariant mass, $\sqrt{\hat{s}}(\mu^+\mu^-)$, which will not be present for the case of initial state radiation.

Figure 6 shows an example of the achievable statistics, possible with the design LHC yearly integrated luminosity of 100 fb^{-1} at 14 TeV, for fully simulated events at the generator level, including the effects of initial and final state radiation and the effects of the smearing of the muon momentum to simulate the finite detector resolution. In particular, it can be seen that the general features of the KK signal discussed earlier remain visible under these conditions. Moreover, it is expected that the deviations from the Standard Model expectation in the $\sqrt{\hat{s}}(\mu^+\mu^-)$ and $p_T(\mu)$ distributions will be sufficient to suggest

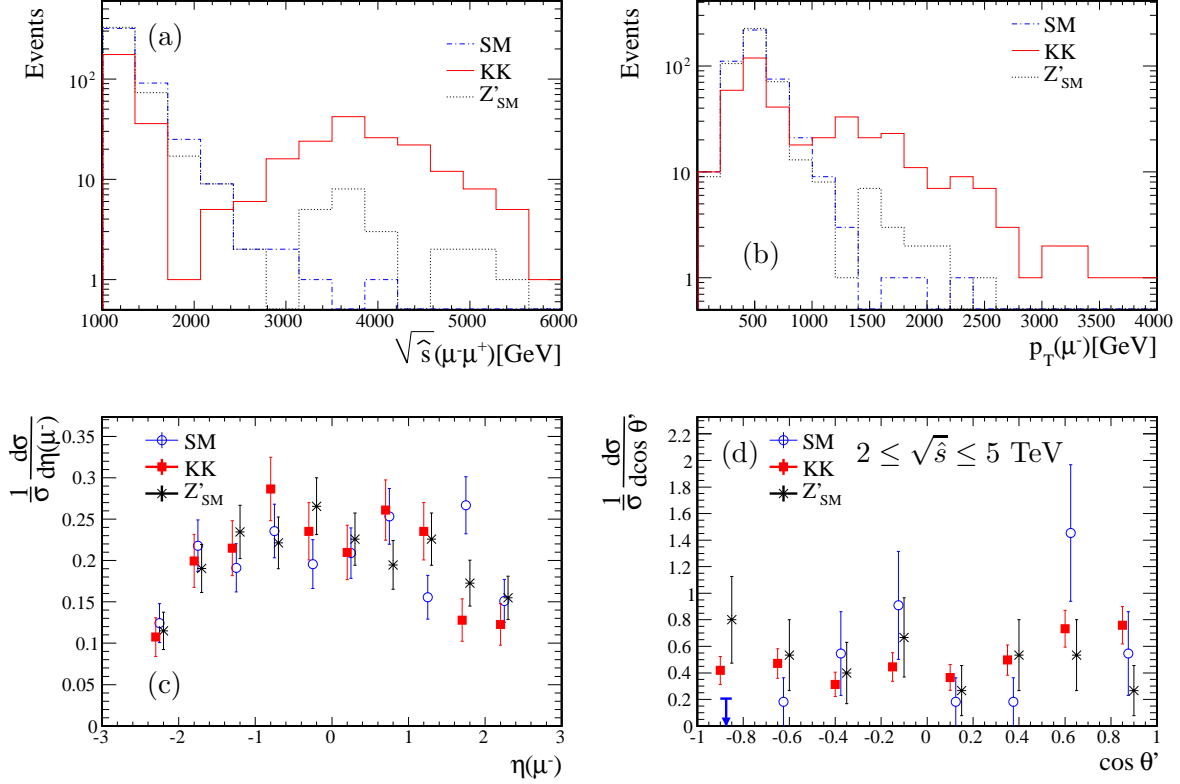


Figure 6: Kinematic distributions for an integrated luminosity, $\mathcal{L}_{LHC}=100 \text{ fb}^{-1}$ for the KK (solid), the SM (dash-dot) and the Z'_{SM} (dotted) models; (a) The di-muon invariant mass, $\sqrt{\hat{s}}(\mu^+\mu^-)$, (b) the muon transverse momentum, p_T , (c) the normalised muon η and, (d) the normalized muons $\cos \theta'$ distributions. The additional requirement of $2 \leq \sqrt{\hat{s}}(\mu^+\mu^-) \leq 5$ TeV has been applied to the events in (d) as in figure 3. Note in (d), the empty bin for the Standard Model distribution at $\cos \theta'$ of -0.9. The length of the arrow in this case represents the 1σ Poisson upper limit.

the existence of a KK resonance even if the mass of the resonance is beyond the reach of the LHC.

4. The LHC sensitivity for the KK signal

The design luminosity and centre-of-mass energy of the LHC are not expected to be achieved before the 2012-2013 shutdown. This imposes strong limitations on the discovery and identification potential at the TeV scale for the first few years of LHC operation. For the early LHC running period, the distributions for the variables seen in figure 6 for $\sqrt{s}_{LHC}=14$ TeV and $\mathcal{L}_{LHC}=100 \text{ fb}^{-1}$ will be significantly different. Even during early LHC operation however, it might be possible to observe, at lower masses, the remote shadow that a much heavier KK state casts in the foothills of the resonance. The current bound on m^* is around 4 TeV, obtained by indirect methods [21], but for completeness, masses lower than this have also been considered for this study.

To study the discovery potential for early LHC running scenarios, the naïve significance for observing the KK peak and the characteristic dip at invariant masses be-

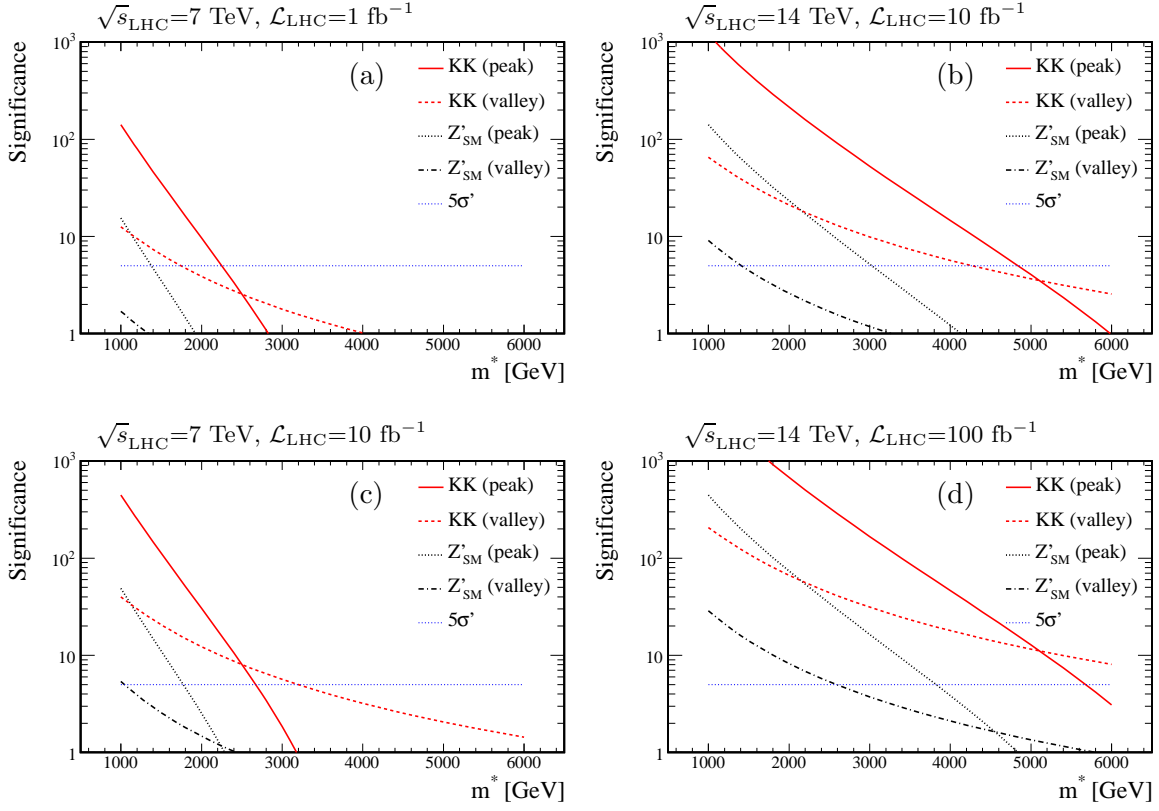


Figure 7: The expected significance for observing events around the first KK peak (solid-red) or in the first KK valley region (red-dashed) as a function of the BSM mass parameter, calculated using equation 4.1 and after an overall K-factor of 1.25 has been applied, the effect of which is to improve the mass reach by transposing the significance curves approximately 50 GeV towards higher masses with respect to the significance without applying this factor. Also shown is the expected significance for the the Z'_{SM} model calculated in the KK peak (black-dotted) and valley (black-dash-dotted) regions, also calculated after applying the 1.25 K-factor. For illustration, the horizontal 5σ line (thin-blue-dotted) is also shown.

low the resonance has been studied. The LHC centre-of-mass energies considered were $\sqrt{s}_{\text{LHC}}=7$ TeV and $\sqrt{s}_{\text{LHC}}=14$ TeV with integrated luminosities in the range $\mathcal{L}_{\text{LHC}}=1$ fb $^{-1}$ to $\mathcal{L}_{\text{LHC}}=100$ fb $^{-1}$. For each LHC configuration the significance, $S(m^*)$, for observing either the peak or the valley, defined by

$$S(m^*) = \frac{|N_{\text{BSM}}(m^*) - N_{\text{SM}}|}{\sqrt{N_{\text{SM}}}}, \quad (4.1)$$

was calculated for various values of m^* , where N_{BSM} and N_{SM} are the number of expected beyond-the-SM and SM events, and where BSM stands for either KK or Z'_{SM} . For this calculation, an overall K-factor of 1.25 has been applied to both the BSM and SM cross section.

The unique form of the KK line shape enables the strict definition of integration ranges for different values of m^* . This feature is present throughout the entire KK tower, where the n^{th} KK peak will always be at $\sqrt{s} \simeq nm^*$ between $m^*(n - \frac{1}{2})$ and $m^*(n + \frac{1}{2})$. As

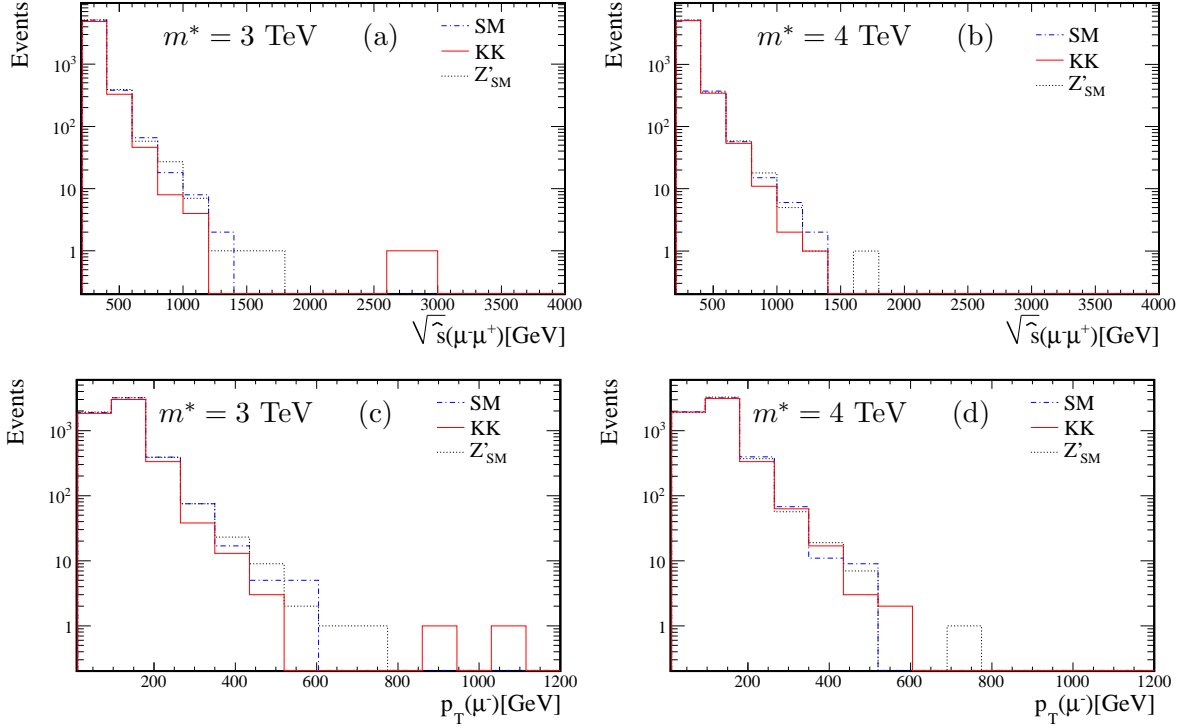


Figure 8: Expected distributions corresponding to $\sqrt{s}_{\text{LHC}}=7$ TeV and $\mathcal{L}_{\text{LHC}}=10$ fb $^{-1}$ for the KK (red, solid), the Standard Model (blue, dash-dot) and the Z'_{SM} (black, dotted) models, as a function of the di-muon invariant mass, $\sqrt{\hat{s}}(\mu^+\mu^-)$, for the two cases of mass parameter, $m^* = 3$ TeV (a) and $m^* = 4$ TeV (b), and as a function of the muon transverse momentum, $p_T(\mu^-)$, also for $m^* = 3$ TeV (c) and $m^* = 4$ TeV (d).

such, the expected number of events for a given integrated luminosity can be calculated by integrating over the invariant mass distributions in either of two mass ranges;

- the KK peak region; $\frac{1}{2}m^* \leq \sqrt{\hat{s}}(\mu^+\mu^-) \leq \frac{3}{2}m^*$, *ie.* between the first two adjacent KK local minima on either side of the first KK mode,
- the KK valley region; $2m_{Z^0} \lesssim \sqrt{\hat{s}}(\mu^+\mu^-) \leq \frac{1}{2}m^*$, *ie.* from approximately ~ 200 GeV up to the first KK local minimum.

In figure 7, the significance in these peak and valley regions is shown as a function of the BSM mass. For illustration the 5σ limit is also shown. Within the models studied here, it can be seen that the significance for the Kaluza-Klein model is always larger than that of the Z'_{SM} model, as would be expected from the smaller signal.

There are two cases where the significance is above 5σ level and is higher for the KK valley region than for the KK peak region. These are

1. $\sqrt{s}_{\text{LHC}}=7$ TeV, $\mathcal{L}_{\text{LHC}}=10$ fb $^{-1}$ and for $2.5 \lesssim m^* \lesssim 3$ TeV.
2. $\sqrt{s}_{\text{LHC}}=14$ TeV, $\mathcal{L}_{\text{LHC}}=100$ fb $^{-1}$ and for $m^* \gtrsim 5$ TeV,

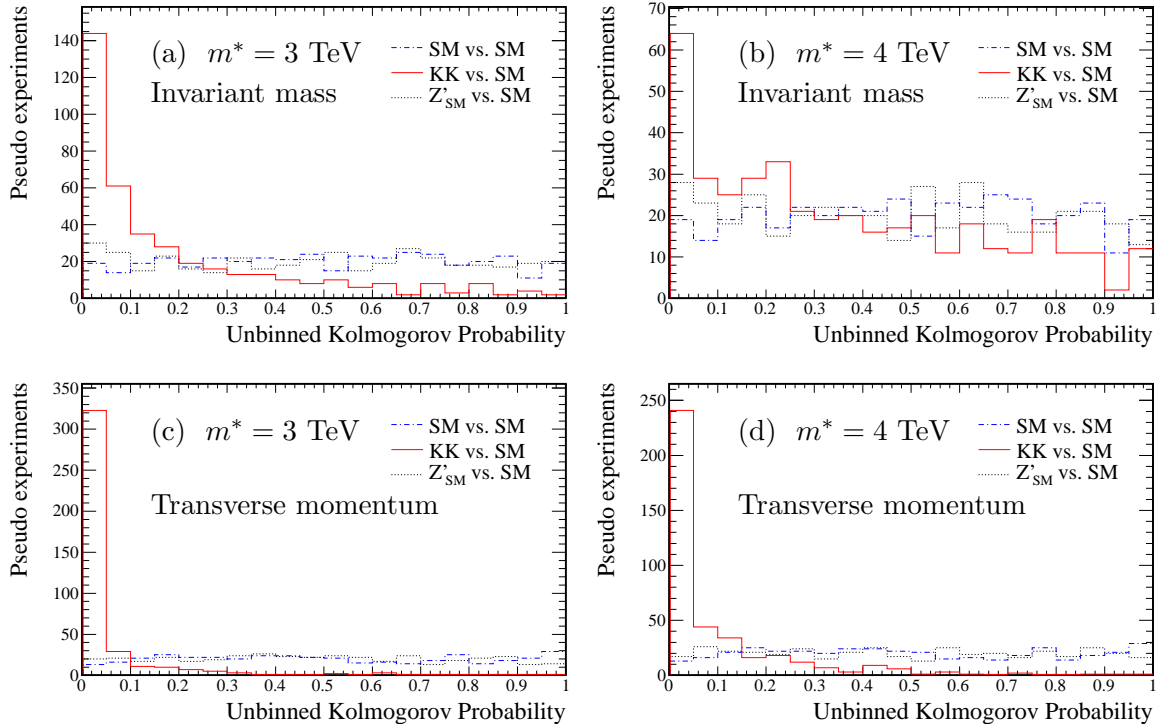


Figure 9: The distribution of the probabilities of the Kolmogorov statistic for comparison between the data from the 400 pseudo-experiments with that from a large reference sample of SM events for the three models, SM (blue, dot-dashed); KK (solid, red); Z'_{SM} (black, dashed). (a) The distribution for the comparison of the invariant mass distribution with $m^* = 3$ TeV, (b) the invariant mass distribution with $m^* = 4$ TeV, (c) and (d) the distributions for the comparison of the muon transverse momentum distribution with $m^* = 3$ TeV and $m^* = 4$ TeV respectively.

whereas for all other cases, the significance of the KK peak region is larger. This indicates that even when the mass of the KK state is beyond the kinematic limit and cannot be observed directly, the suppression of the cross section at lower invariant masses may still provide useful information.

However, in the integration over the invariant mass distribution, without a sensitive choice of the limits of the integration which are not *a priori* known, there will be some cancellation between the number of events from the peak and the valley regions which may reduce the apparent significance.

A more sensitive method in this case may be to use the shape of the invariant mass distribution itself rather than obtain N_{BSM} and N_{SM} by integrating over some unknown peak and valley regions. This might be most useful for the data from the first few years of LHC operation where both the beam energy and luminosity will be lower. In such a case, although a resonance itself might not be observed, the first signs of a faster than expected fall of the cross section may provide an indication of a signal in the TeV region.

To ascertain the likely potential for discrimination between the various models using the early LHC data, data from 400 pseudo-experiments was generated with three datasets per pseudo-experiment - one each for the Standard Model, the KK and Z'_{SM} models, in-

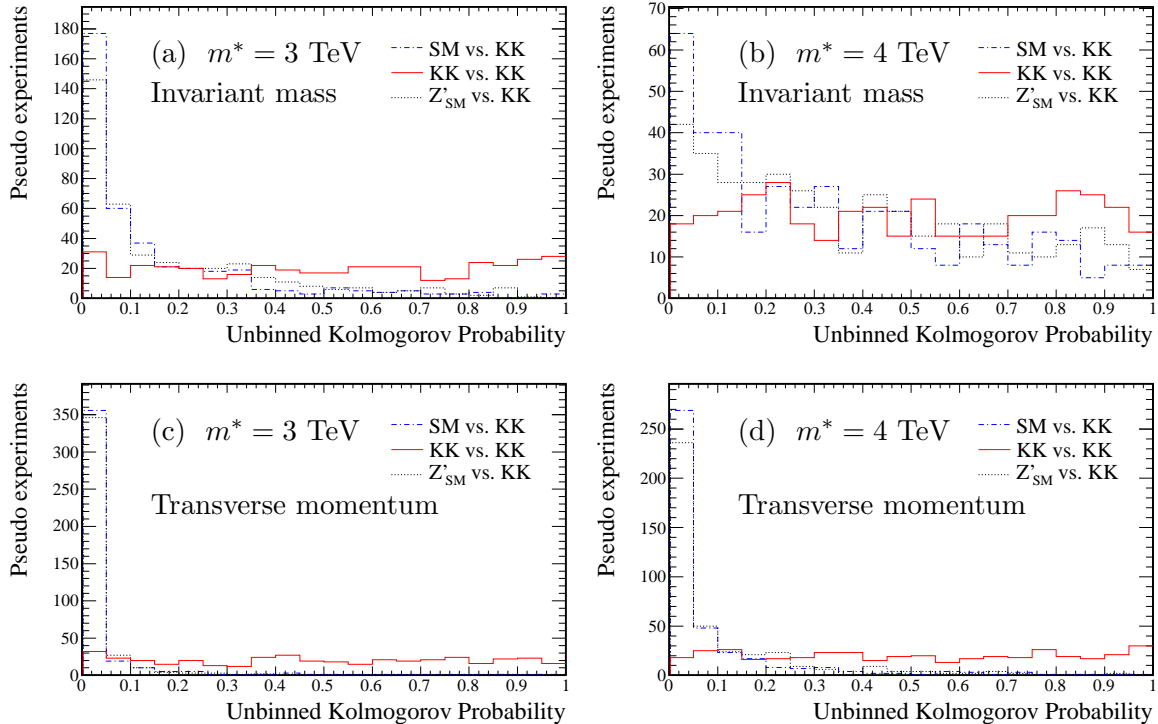


Figure 10: The distribution of the probabilities of the Kolmogorov statistic for comparison between the data from the 400 pseudo-experiments with that from a large reference sample of KK events for the three models, SM (blue, dot-dashed); KK (solid, red); Z'_{SM} (black, dashed). (a) The distribution for the comparison of the invariant mass distribution with $m^* = 3$ TeV, (b) the invariant mass distribution with $m^* = 4$ TeV, (c) and (d) the distributions for the comparison of the muon transverse momentum distribution with $m^* = 3$ TeV and $m^* = 4$ TeV respectively.

cluding the muon transverse momentum smearing to simulate the effects of finite detector resolution. An analysis comparing the results of each pseudo-experiment to a large reference sample was performed using the reconstructed $\mu^+\mu^-$ invariant mass and the observed muon transverse momentum distributions. Figure 8 illustrates the distributions for the data from a single pseudo-experiment for the case of $\sqrt{s}_{LHC}=7$ TeV and $\mathcal{L}_{LHC}=10$ fb $^{-1}$ and two possible values of $m^* = 3$ TeV and $m^* = 4$ TeV.

In figure 9 the results of an unbinned Kolmogorov probability comparison of the three data sets in each pseudo-experiment with a large SM reference sample is presented for the invariant mass distribution and for the transverse momentum distribution of the leading muon. Each comparison has been performed for pseudo-data samples with $m^* = 3$ TeV and $m^* = 4$ TeV. For the distributions used for these comparisons, the leading order cross sections have been assumed. Since the NLO K-factor of 1.25 would predict a larger cross section than the LO cross section presented, this might suggest a small increase in both the statistical precision and discrimination between the various signals would be possible with actual data, and as such the results presented here should be considered as a conservative estimate.

In all four distributions from figure 9 the probability for obtaining the Kolmogorov

statistic when comparing the small SM pseudo-datasets with the large SM sample is flat, as expected for compatible data sets, as is that for the Z'_{SM} model. The comparison of the KK signal is however, quite heavily peaked at lower probabilities, being most significant for the transverse momentum distribution, most notably for the $m^* = 3$ TeV scale.

Similarly, figure 10 shows the same comparison of the three data sets for each pseudo-experiment, but this time compared to a large sample of KK events. In this case, the distributions of probabilities from comparing the KK samples are flat, again as expected for compatible distributions, whereas both the SM and Z'_{SM} samples are peaked at lower probabilities.

Model	m^*	$\sqrt{\hat{s}}$ distributions	p_T distributions
Z'_{SM}	3 TeV	0.075	0.05
Z'_{SM}	4 TeV	0.07	0.043
KK	3 TeV	0.36	0.81
KK	4 TeV	0.16	0.6

Table 1: Probabilities for excluding, within a 95% confidence level the SM given the observed distributions from the KK and Z'_{SM} samples.

This indicates a potentially observable incompatibility between the KK pseudo-experiments and the large SM reference sample. The probabilities to exclude the SM hypothesis with a 95% confidence level for the KK or Z'_{SM} samples presented here can be seen in table 1. The probabilities to exclude the KK hypothesis with a 95% confidence level given the SM or Z'_{SM} models are presented in table 2.

Model	m^*	$\sqrt{\hat{s}}$ distributions	p_T distributions
Z'_{SM}	3 TeV	0.37	0.87
Z'_{SM}	4 TeV	0.11	0.59
SM	(KK, 3 TeV)	0.44	0.89
SM	(KK, 4 TeV)	0.16	0.67

Table 2: Probabilities for excluding, within a 95% confidence level, the KK given the observed distributions from the KK and Z'_{SM} samples.

This suggests that even with the reduced luminosity and centre-of-mass energy available during the early LHC running, it may still be possible to distinguish a low mass KK signal from both the Standard Model, and a Z'_{SM} signal similar to that studied.

5. Summary and Outlook

The hard process for simulating the tower of Kaluza-Klein electroweak boson exchange within the S^1/Z_2 extra dimensional model has been independently verified, and implemented in the MOSES framework and integrated with the PYTHIA8 generator. The process itself is also now included [29] in the most recent release of PYTHIA8. This process is particularly interesting in the context of the early LHC programme of operation since it features several signatures that might enable the observation of a significant departure from the

corresponding Standard Model expectation. A preliminary study considering the observation of evidence for a resonance inside or just beyond the kinematic reach of the LHC has been performed for the early LHC running scenario, and suggests that for a Kaluza-Klein resonance above 3 TeV such an observation may still be possible with early LHC data, whereas for a model based on the Z'_{SM} such an observation in the same mass range may not be possible.

6. Acknowledgments

The authors would like to acknowledge the financial support of the Israeli Science Foundation, the United Kingdom Science and Technology Facilities Council and the MCnet programme. Personal thanks are given to Mike Seymour and Jonathan Butterworth for supporting the work on the MOSES framework. Special thanks are given to the PYTHIA authors, Torbjörn Sjöstrand and Stefan Ask for useful discussions and advice on the integration of the discussed KK hard process within the PYTHIA8 framework. The authors would also like to thank Evgeny Yurkovsky and Tom Rizzo for fruitful discussions.

References

- [1] N. Arkani-Hamed, S. Dimopoulos and G. R. Dvali, *Phys. Lett.* **B 429** (1998) 263; N. Arkani-Hamed, S. Dimopoulos and G. R. Dvali, *Phys. Rev.* **D 59** (1999) 086004.
- [2] I. Antoniadis, *Phys. Lett.* **B 246** (1990) 377; I. Antoniadis, *J. of Phys.* Conference Series 33 and references therein (2006).
- [3] L. Randall and R. Sundrum, *Phys. Rev. Lett.* **83** (1990) 3370; L. Randall and M. D. Schwartz, *Phys. Rev. Lett.* **88** (2002) 081801; L. Randall and M. D. Schwartz, *J. High Energy Phys.* **0111** (2001) 003.
- [4] K. R. Dienes, E. Dudas and T. Gherghetta, *Phys. Lett.* **B 436** (1998) 55; K. R. Dienes, E. Dudas and T. Gherghetta, *Nucl. Phys.* **B 537** (1999) 47.
- [5] A. Pomarol, M. Quiros, *Phys. Lett.* **B 438** (1998) 255; M. Masip, A. Pomarol, *Phys. Rev.* **D 60** (1999) 096005; I. Antoniadis, K. Benakli, M. Quiros *Phys. Lett.* **B 460** (1999) 176.
- [6] N. Arkani-Hamed and M. Schmaltz, *Phys. Rev.* **D 61** (2000) 033005.
- [7] L. Evans, (ed.), P. Bryant, (ed.), *JINST* **3** (2008) S08001.
- [8] A. Leike, 1999 *Phys. Rep.* **317** 143.
- [9] T. G. Rizzo, *Phys. Rev.* **D 61** (2000) 055005.
- [10] T. G. Rizzo, *J. High Energy Phys.* **08** (2009) 082.
- [11] G. Bella, E. Etzion, N. Hod and M.R. Sutton, (2010) <http://projects.hepforge.org/moses>, arXiv:1004.1649.
- [12] T. Sjöstrand, S. Mrenna and P. Skands, 2007 “A brief introduction to PYTHIA 8.1”, arXiv:0710.3820.
- [13] F. del Aguila, *Acta Phys. Polon.* **B25** (1994) 1317.
- [14] G. Azuelos and G. Polesello, *Eur. Phys. J.* **C 39** (2004) s2, s1–s11.

- [15] E. Richter-Was, D. Froidevaux, L. Poggioli, ATLAS Internal Note ATL-PHYS-96-079 (1996);
E. Richter-Was, D. Froidevaux, L. Poggioli, ATLAS Internal Note ATL-PHYS-98-131 (1998).
- [16] The ATLAS Collaboration, JINST **3** (2008) S08003.
- [17] M. Dittmar, A. S. Nicollerat and A. Djouadi, *Phys. Lett.* **B 583** (2004) 111.
- [18] D. Bardin *et al.* CERN-TH.5468/89 (1989).
- [19] T. G. Rizzo, SLAC-PUB-10753 (2004); T. G. Rizzo, SSI-2004-L013 (2004).
- [20] K. Cheung and G. Landsberg, *Phys. Rev.* **D 65** (2002) 076003; J. Hewett and M. Spiropulu, 2002 *Annu. Rev. Nucl. Part. Phys.* **Vol 22**.
- [21] C. Amsler *et al* (Particle Data Group) *Phys. Lett.* **B 667** (2008) volume. C. Amsler *et al* (Particle Data Group) 2009 partial update for the 2010 edition.
- [22] E. Yurkovsky, “Prospects for Kaluza-Klein Excitations Search in the Di-Lepton Channel at the LHC” CERN-THESIS-2010-036 (2010).
- [23] T. G. Rizzo, SLAC-PUB-12129, (2006) hep-ph/0610104.
- [24] F. Petriello and S. Quackenbush, *Phys. Rev.* **D 77** (2008) 115004.
- [25] J. Collins and D. E. Soper, *Phys. Rev.* **D 16** (1977) 2219.
- [26] A. D. Martin, R. G. Roberts, W. J. Stirling and R. S. Thorne, *Eur. Phys. J.* **C 23** (2001) 73;
A. D. Martin, R. G. Roberts, W. J. Stirling and R. S. Thorne, *Phys. Lett.* **B 531** (2002) 216.
- [27] The ATLAS Collaboration, “Expected Performance of the ATLAS Experiment, Detector, Trigger and Physics” CERN-OPEN-2008-020 (2010).
- [28] S. Lacaprara, *Eur. Phys. J.* **C 34** (2004) s75.
- [29] T. Sjöstrand, private communication.